

Magnetic braking and damping of differential rotation in massive starsLunan Sun,¹ Milton Ruiz,¹ and Stuart L. Shapiro^{1,2}¹*Department of Physics, University of Illinois at Urbana-Champaign, Urbana, Illinois 61801, USA*²*Department of Astronomy & NCSA, University of Illinois at Urbana-Champaign, Urbana, Illinois 61801, USA*

(Received 6 December 2018; published 29 March 2019)

Fragmentation of highly differentially rotating massive stars that undergo collapse has been suggested as a possible channel for binary black hole formation. Such a scenario could explain the formation of the new population of massive black holes detected by the LIGO/VIRGO gravitational wave laser interferometers. We probe that scenario by performing general relativistic magnetohydrodynamic simulations of differentially rotating massive stars supported by thermal radiation pressure plus a gas pressure perturbation. The stars are initially threaded by a dynamically weak, poloidal magnetic field confined to the stellar interior. We find that magnetic braking and turbulent viscous damping via magnetic winding and the magneto-rotational instability in the bulk of the star redistribute angular momentum, damp differential rotation and induce the formation of a massive and nearly uniformly rotating inner core surrounded by a Keplerian envelope. The core + disk configuration evolves on a secular timescale and remains in quasistationary equilibrium until the termination of our simulations. Our results suggest that the high degree of differential rotation required for $m = 2$ seed density perturbations to trigger gas fragmentation and binary black hole formation is likely to be suppressed during the normal lifetime of the star prior to evolving to the point of dynamical instability to collapse. Other cataclysmic events, such as stellar mergers leading to collapse, may therefore be necessary to reestablish sufficient differential rotation and density perturbations to drive nonaxisymmetric modes leading to binary black hole formation.

DOI: [10.1103/PhysRevD.99.064057](https://doi.org/10.1103/PhysRevD.99.064057)**I. INTRODUCTION**

The multiple detections by the LIGO/VIRGO Scientific Collaboration (LVSC) of gravitational wave (GW) signals produced by binary black hole (BH) mergers [1–6] provides the clearest evidence of the existence and common occurrence of close binary BHs. These detections also point to a new population of stellar-mass binary BHs whose masses are larger than those of the twenty x-ray BH binaries with masses $\lesssim 20 M_{\odot}$ [7], and it raises a puzzle regarding the origin of these massive BH binaries.

There are various scenarios proposed to explain the formation of massive BH binaries, such as the coalescence of primordial black holes [8–11] and failed supernova explosion [12]. The collapse of a massive star ($M \gtrsim 10 M_{\odot}$) has been suggested as one of the most plausible formation channels for BHs observed by the LVSC [12–14]. As the final mass of the BH remnant depends sensitively on the mass and metallicity of the progenitor stars [15], it is somehow expected that the direct-collapse of Population III (Pop III) stars form the most massive BHs [16,17]. This hypothesis was confirmed by population synthesis simulations of Pop III stars [18], where binary BHs with typical mass of $\sim 30 M_{\odot}$ were formed from 10^6 Pop III binary evolutions with masses ranging between $10 M_{\odot}$ to $100 M_{\odot}$. The study in [19]

suggests that a binary containing massive stars with masses $M_1 \approx 96 M_{\odot}$ and $M_2 \approx 60 M_{\odot}$ at redshift $z \approx 3.2$ may be the progenitor of the first BH binary detected by the LVSC (event GW150914) [1]. Later, it was shown in [20] that the events GW150914 and GW151226, as well as the lower-confidence event LVT151012, may be explained by the isolated binary evolution channel (i.e., assuming that the binary never interacts with another star) from progenitor stellar binaries with masses between $60 M_{\odot} - 160 M_{\odot}$. This channel involves the formation of a common envelope through which mass is transferred between the secondary star and its companion via stellar winds. However, such a common-envelope phase is not well understood and results in great physical uncertainties for the BH formation rate due to the lack of observational evidence [21]. To avoid this phase, an evolution channel including massive overcontact binaries, where two tightly bound stars are sufficiently mixed due to their tidally induced high spin, has been considered [22]. Prior to collapse, the massive close binary components are fully mixed and achieve chemical homogeneity. As the hydrogen burning ends nearly simultaneously for the two binary components, the post-main-sequence expansion is suppressed due to the absence of a hydrogen-rich envelope. According to the mass exchange mechanism, this evolution route is therefore likely to

produce BH binaries with a large mass ratio, as in GW150914 [23].

It also has been suggested that stellar-massive BHs can be formed via dynamical interactions in dense clusters. In clusters with low metallicities, such as the cores of globular clusters (GCs) or dense AGNs [24] it is possible to form binary systems dynamically via gravitational interactions among a population of stellar-mass BHs [25,26] or hierarchical mergers of smaller BHs [27]. In particular, a simulation of GCs of mass $M \sim 10^5 - 10^6 M_\odot$ with many-body dynamics and stellar evolution has provided an evolutionary channel for BH binaries similar to GW150914 [28]. It is expected that the two mechanisms described above can be distinguished by the binary spins from a large, future sample of BH mergers. The BH binaries formed from direct collapse of massive stars are more likely to result in aligned spins due to tidal interactions and/or mass transfer, while dynamically formed binaries will have randomly oriented spins. In addition, the further merging of the massive BH remnants in GCs may finally form more massive intermediate-mass black holes (IMBHs), defined as BHs with mass $10^2 - 10^5 M_\odot$ [29]. An all-sky survey of GW signals from binary IMBHs has been performed by LVSC. For such systems, the merger rate is constrained to be $\gtrsim 0.3 \text{ GC}^{-1} \text{ Gyr}^{-1}$ in the local Universe with 90% confidence [30]. Other evolution channels, such as the direct collapse of very massive Pop III stars, can also form IMBHs [29,31].

Among the binary BH detections by LVSC, GW150914 and GW170104 are possibly associated with electromagnetic (EM) counterparts [32,33]. Although the EM emission is unexpected for binary BHs mergers in pure vacuum (see e.g., [34]), in these two events, gamma-ray signals with isotropic energy $\sim 10^{49} - 10^{50}$ erg have been observed shortly after the peak GW signals [32,33]. With the assumption that the EM transient is connected to the GW events, fully general relativistic magnetohydrodynamic (GRMHD) simulations in [35] show that magnetized disk accretion onto a BH binary could explain GW and EM counterparts such as the GBM hard x-ray signal reported 0.4s after GW150914. Massive star fragmentation during gravitational collapse has been proposed as an alternative scenario [36]. However, numerical simulations and analytic studies have shown that binary BHs coalescence within a dense stellar gas ($\rho \gtrsim 10^7 \text{ g cm}^{-3}$) produces a waveform different from one in vacuum due to gas drag [37,38]. To rectify this effect, the single-progenitor scenario with an accretion rate $\sim 3 \times 10^9$ times the Eddington rate prior to merger has been suggested [39]. This so-called giga-Eddington accretion can drive out the stellar gas as well as alter the time delay between GW and EM signals. However, that scenario may not account for all the physical processes involved, in particular magnetically-driven processes (see e.g.,

[35,40,41]), which can have a dynamical impact on the evolution channel.

Returning to the collapse of massive stars as the origin of massive BHs and massive BH binaries, we note that massive stars are radiation dominated and well-approximated by an $n \sim 3$ ($\Gamma \sim 4/3$) polytrope. During their evolution, very massive (and supermassive) stars cool and contract until they ultimately encounter a relativistic, dynamical instability leading to catastrophic collapse to BHs (see [42–48]). Massive stars that are *uniformly* rotating remain nearly axisymmetric during the collapse, as shown by post-Newtonian [44] and fully general relativistic (GR) simulations [49,50]. However, massive stars that are *differentially* rotating with a sufficiently high ratio of rotational kinetic energy to gravitational potential energy ($T/|W| \gtrsim 0.14$) are secularly unstable to forming $m = 2$ bar modes during the course of their evolution [51–53]. In addition, differentially rotating massive stars with non-axisymmetric (e.g., bar mode) density perturbations and undergoing collapse can fragment into self-gravitating, collapsing components that form seed BHs [45,54]. In some cases, this fragmentation may lead to the formation of massive BH binaries [55].

Even though intensive studies of the evolution channels and the interactions of collapsing massive stars have been studied previously, our understanding of the role of the magnetically driven instabilities during their stellar evolution prior to collapse remains poor.

Newtonian simulations of magnetic braking (i.e., winding) and viscous damping of an incompressible, differentially rotating infinite cylinder model were performed in [56]. It was found that differential rotation could generate toroidal Alfvén waves that convert an appreciable fraction of rotational kinetic energy to magnetic energy and drive the star toward uniform rotation (“magnetic braking”). The destruction of differential rotation was also demonstrated later on in a compressible cylinder model [57] and in relativistic, neutron star models, both incompressible [58] and compressible [59]. The role of turbulent viscosity in damping differential rotation in rapidly spinning, neutron stars obeying a “stiff” ($\Gamma = 2$) equation of state (EOS) was demonstrated by simulations in axisymmetry in [60], where the Navier-Stokes equations with a shear viscosity were solved in full GR. They found that the viscosity drives the neutron stars to a high density, uniformly rotating core surrounded by a Keplerian disk in which the core could either collapse to a BH or remain stable depending on its mass and the viscous build-up of thermal pressure. Subsequently, the role of magnetic fields in driving viscous turbulence via the magneto-rotational instability (MRI), which damps the differential rotation in a hypermassive neutron star, was demonstrated by GRMHD simulations in axisymmetry in [59,61–63]. They showed that the magnetic energy is amplified both by the winding

of field lines and MRI, and that the differential rotation is significantly reduced due to the magnetic braking and MRI-induced turbulent viscous damping.

In this paper, we explore this braking and damping scenario in weakly magnetized, differentially rotating massive stars in hydrostatic equilibrium. In particular, we perform GRMHD simulations to probe the effects of magnetic winding and magnetic-induced turbulent viscosity that can break the differential rotation in massive stars. We consider massive stars governed by a soft $n \lesssim 3$ ($\Gamma \gtrsim 4/3$) EOS. We first show that, for magnetized stars with characteristic masses greater than several hundred M_\odot , the hierarchy of physical timescales meets the criteria for the magnetic damping of differential rotation within stellar lifetimes. Then we construct stable equilibrium stars with the same differentially rotating profiles as in the initial (collapsing) configurations employed in [55], where fragmentation of $m = 2$ seed density perturbations into BH binaries occurs. We endow the stars with a dynamically weak, dipole magnetic field confined to the stellar interior and evolve the resulting magnetized equilibrium configuration in $3 + 1$ dimensions using our Illinois GRMHD code. We find that well prior to collapse, magnetic braking and turbulent viscosity induces the formation of an inner core surrounded by a thick, Keplerian, circumstellar disk after several Alfvén timescales. As anticipated, magnetic braking, induced by the toroidal winding of the magnetic field, and viscous damping, induced by magnetic turbulence triggered by the MRI, drive the inner core to uniform rotation. The newborn core + disk configuration evolves on a secular (viscous) timescale and remains in quasistationary equilibrium until we terminate the simulations. Our results suggest that *a stellar fragmentation scenario for a massive star that evolves in isolation is not a plausible formation channel for binary BHs*. Other cataclysmic events, such as the merger of two massive stars, may be necessary to reestablish sufficient differential rotation to drive nonaxisymmetric modes leading to fragmentation of a dynamically unstable remnant into binaries during collapse. Our results apply for stars prior to BH formation with characteristic masses greater than several hundred solar masses. The masses in our simulations are chosen for demonstration purposes and were selected for their microphysical simplicity and computational practicality. However, we do expect qualitative similar outcomes to apply for lower masses relevant to the LIGO/Virgo BH progenitors.

The structure of the remainder of the paper is as follows. In Sec. II, we calculate several key physical timescales and show that the hierarchy of timescales for plausible initial configurations satisfy conditions inevitably leading to the magnetic destruction of differential rotation. In Sec. III, we discuss the properties of typical initial configurations and describe the initial models used

in our simulations. In Sec. IV, we describe the numerical tools we use, the numerical implementation of the initial data and evolution, and some of the diagnostics employed to verify the reliability of our simulations. We summarize our results and compare them with previous work in Sec. V. Finally, we offer conclusions in Sec. VI. We adopt geometrized units ($G = c = 1$) throughout the paper except where stated explicitly. Greek indices denote all four spacetime dimensions, while Latin indices imply spatial parts only.

II. TIMESCALES

There are four important timescales related to the evolution of magnetized, differentially rotating, massive stars:

- (1) The *dynamical timescale* t_{dyn} determines the rate of collapse (“free-fall”) of the star to a BH after the onset of dynamical radial instability. It is also the timescale for a perturbed, stable star to relax to hydrostatic equilibrium. In order to guarantee that the star maintains hydrostatic equilibrium while undergoing magnetic braking or other secular perturbations, t_{dyn} must be shorter than these other timescales.
- (2) The *Alfvén timescale* t_A is the winding timescale of a poloidal magnetic field in a differentially rotating star [56]. The magnetic braking of differential rotation usually requires several changes in the direction of magnetic field rotation, therefore t_A is an appreciable fraction of the total braking timescale.
- (3) The *viscous timescale* t_{vis} represents the time over which the turbulent viscosity, induced by magnetic field instabilities, damps differential rotation.
- (4) The *thermal timescale* t_{th} determines the lifetime of a very massive star, which radiates at the Eddington limit. This timescale must be longer than the above timescales in order for the magnetic braking and damping of differential rotation to be completed during the lifetime of a stable star.

The above timescales depend on various factors such as the equation of state, radius, degree of differential rotation, and initial magnetic field strength. In a polytrope, they can be described approximately by several parameters: polytropic index n , typical density ρ , characteristic mass M , compaction $\mathcal{C} \equiv M/R$, where R is the characteristic radius, and the ratio of magnetic energy to gravitational potential energy $\mathcal{M}/|W|$. To establish the physical hierarchy of timescales, we scale the parameters above as in our canonical model **N29** (see Table I). In addition, we scale our estimates to a characteristic mass of $10^4 M_\odot$ following our analysis of an $n = 2.9$ polytrope at the onset of collapse in [50]. Since the ratio of rotational kinetic energy to gravitational potential energy $T/|W| \ll 1$, we can use spherical models in making our rough analytic estimates. So, the above timescales can be estimated as follows:

TABLE I. Initial model parameters. Here n denotes the polytropic index, M is the characteristic mass, \bar{M}_{ADM} is the ADM mass, $\bar{\rho}_c$ is the rest-mass central density, R_{pol} is the polar radius, \bar{J}_{ADM} is the ADM angular momentum, $\mathcal{M}/|W|$ denotes the ratio of magnetic energy to gravitational potential energy, and $T/|W|$ the ratio of rotational kinetic energy to gravitational potential energy. In these cases we have set $\bar{\mathcal{M}} = 3.711 \times 10^{-6}$.^d

Case	n	M/M_{\odot}	\bar{M}_{ADM} ^a	$\bar{\rho}_c$ ^b	$R_{\text{pol}}/M_{\text{ADM}}$	\bar{J}_{ADM} ^c	$\mathcal{M}/ W $	$T/ W $
N29	2.9	$\sim 10^4$	4.139	4×10^{-8}	161	36.92	1.88×10^{-4}	0.091
N295	2.95	$\sim 10^5$	4.801	2×10^{-8}	192	52.44	1.82×10^{-4}	0.085

^a $\bar{M}_{\text{ADM}} = K^{-n/2} M_{\text{ADM}}$ where $K = P/\rho_0^\Gamma$.

^b $\bar{\rho}_c = K^n \rho_c$.

^c $\bar{J}_{\text{ADM}} = K^{n/2} J_{\text{ADM}}$.

^d $\bar{\mathcal{M}} = K^{-n/2} \mathcal{M}$, Nondimensional quantities have been rescaled with the polytropic gas constant K and are denoted with a bar.

(1) The *dynamical timescale* is

$$t_{\text{dyn}} \sim \langle \rho \rangle^{-1/2} \sim \left(\frac{M}{R} \right)^{-3/2} M$$

$$\sim 10^2 \left(\frac{M}{10^4 M_{\odot}} \right) \left(\frac{C}{6 \times 10^{-3}} \right)^{-3/2} \text{ s.} \quad (1)$$

(2) The *Alfvén timescale* can be calculated as

$$t_A \sim R/v_A$$

$$\sim 10^4 \left(\frac{\mathcal{M}/|W|}{2 \times 10^{-4}} \right)^{-1/2} \left(\frac{M}{10^4 M_{\odot}} \right) \left(\frac{C}{6 \times 10^3} \right)^{-3/2} \text{ s,} \quad (2)$$

where $v_A = B/\sqrt{4\pi\rho}$ is the Alfvén speed and ρ is the characteristic density of conducting plasma (here the stellar gas). For our canonical model (see Sec. III), the Alfvén timescale is typically two orders of magnitude longer than the dynamical timescale.

(3) The *viscous timescale* is

$$t_{\text{vis}} \sim \frac{R^2}{\nu} \sim \frac{R}{\alpha_{\text{ss}} c_s}, \quad (3)$$

where $\nu = \alpha_{\text{ss}} H c_s$ is the shear viscosity. Here $c_s = (\partial P/\partial \rho)^{1/2}$ denotes the sound speed. We take the dimension of a viscous vortex H to be comparable to the stellar radius. The quantity α_{ss} denotes the Shakura–Sunyaev α_{ss} -disk parameter computed as (see Eq. 26 in [64])

$$\alpha_{\text{ss}} = \frac{T_{\hat{r}\hat{\phi}}^{\text{EM}}}{P + P_{\text{mag}}} \sim \frac{T_{\hat{r}\hat{\phi}}^{\text{EM}}}{P}, \quad (4)$$

where P is the matter + radiation pressure, P_{mag} is the magnetic pressure, and T^{EM} is the electromagnetic stress energy tensor defined as

$$T_{\mu\nu}^{\text{EM}} = b^2 u_{\mu} u_{\nu} + b^2 g_{\mu\nu}/2 - b_{\mu} b_{\nu}, \quad (5)$$

where $b^{\mu} = B_{(u)}^{\mu}/(4\pi)^{1/2}$ is the magnetic field measured by an observer comoving with the fluid, $b^2 = b^{\mu} b_{\mu}$, and u^{μ} denotes the 4-velocity of the plasma (see [65] for discussion). Using Eq. (5), and the fact that $c_s \sim (P/\rho)^{1/2} \sim (M/R)^{1/2}$, α_{ss} can be estimated as

$$\alpha_{\text{ss}} \sim \frac{B^{\hat{r}} B^{\hat{\phi}}}{P}. \quad (6)$$

Accordingly,

$$t_{\text{vis}} \sim \frac{1}{\alpha_{\text{ss}}} M^{-1/2} R^{3/2} \sim \frac{1}{\alpha_{\text{ss}}} t_{\text{dyn}}. \quad (7)$$

Using Eq. (1) and an effective viscous parameter $\alpha_{\text{ss}} \sim 10^{-4}$, which is the maximum mean value for α_{ss} during our simulations, we obtain

$$t_{\text{vis}} \sim 10^5 \left(\frac{\alpha_{\text{ss}}}{10^{-4}} \right)^{-1} \left(\frac{M}{10^4 M_{\odot}} \right) \left(\frac{C}{6 \times 10^3} \right)^{-3/2} \text{ s,} \quad (8)$$

In our canonical model, the viscous timescale is one order of magnitude longer than the Alfvén timescale [see Eq. (2)]. However, this estimate is very crude due to the local variations of α_{ss} , which may vary by an order of magnitude at different locations.

(4) The *thermal timescale* is defined as

$$t_{\text{th}} \equiv \frac{E_{\text{th}}}{L_{\text{Edd}}}, \quad (9)$$

where E_{th} is the thermal energy of the star and $L_{\text{Edd}} = 4\pi M/\kappa$ is the Eddington luminosity with κ the opacity [42]. The thermal energy can be estimated from the Newtonian virial theorem

$$2T + W + 3(\Gamma - 1)E_{\text{th}} + \mathcal{M} = 0. \quad (10)$$

For small $T/|W|$, $\mathcal{M}/|W|$ and $\Gamma \gtrsim 4/3$, the virial theorem gives

$$W + E_{\text{th}} \approx 0. \quad (11)$$

Therefore, we obtain $E_{\text{th}} \approx |W| \sim M^2/R$, and Eq. (9) becomes

$$t_{\text{th}} \sim 10^{12} \left(\frac{C}{6 \times 10^{-3}} \right) \text{ s} \sim 10^5 \left(\frac{C}{6 \times 10^{-3}} \right) \text{ yrs}, \quad (12)$$

where we have assumed $\kappa = 0.4 \text{ cm}^2 \text{ g}^{-1}$, appropriated for Thomson scattering in a hydrogen gas, and hence $L_{\text{Edd}} \sim 10^{42} (M/10^4 M_{\odot}) \text{ erg s}^{-1}$. In our canonical case **N29** the thermal timescale t_{th} is therefore about $\sim 10^7$ times larger than the viscous timescale [see Eq. (8)].

To achieve the magnetic damping of differential rotation during the stellar lifetime of an equilibrium star prior to reaching the onset of dynamical instability to radial collapse, the evolution of the massive star should satisfy the following hierarchy of timescales

$$t_{\text{dyn}} < t_{\text{A}} < t_{\text{vis}} (\sim t_{\text{damping}}) < t_{\text{th}} (\sim t_{\text{lifetime}}). \quad (13)$$

In particular, the values for case **N29** in Table I provide a model which satisfies this typical hierarchy. In general, stars with several hundred solar masses are radiation dominated and have $2.9 \lesssim n \lesssim 3$ [see Eq. (15) below]. Hence, the hierarchy of timescales in Eq. (13) applies to such stars and strongly suggests that differential rotation will be damped prior to BH formation. This result is demonstrated by our detailed simulation below.

III. INITIAL DATA

To numerically study magnetic braking and damping of differential rotation in massive stars, we consider initial data satisfying the following criteria:

- (1) An EOS dominated by thermal radiation pressure perturbed by thermal gas pressure. We consider a polytropic EOS with $n = 2.9$ and $n = 2.95$ (see Table I).
- (2) Stars in hydrostatic equilibrium with a lifetime longer than the viscosity timescale [see Eq. (8)].
- (3) A small magnetic field to induce magnetic winding and an effective turbulent viscosity. The stars are seeded with a dynamically unimportant poloidal magnetic field ($\mathcal{M}/|W| \sim 10^{-4}$ (See Table I).
- (4) A damping timescale realizable given our computational resources, which requires a significant initial magnetic field, albeit one that is dynamically weak with $\mathcal{M}/|W| \ll 1$. We aim to provide an “existence

proof” for the magnetic braking and damping of differential rotation in massive stars with the finite computational resources at our disposal.

A radiation-dominated stellar model with radiation pressure P_{rad} and a small perturbation due to gas pressure P_{gas} can be described by a polytrope with polytropic index n slightly less than 3 (or equivalently, with adiabatic index Γ slightly greater than $4/3$). In particular, the fraction of gas pressure P_{gas} is quantified by the parameter

$$\beta = P_{\text{gas}}/P_{\text{rad}}. \quad (14)$$

The relation between n (Γ) and the characteristic mass M is given by

$$n \approx \frac{3}{1 + 4.242(M/M_{\odot})^{-1/2}}, \quad (15)$$

which strictly holds for nonrotating, spherical stars. We build rotating equilibrium stellar models using the GR equilibrium code described in [66–68]. We consider two cases for illustrative purposes, choosing two polytropic indices, $n = 2.9$ (case **N29**) and $n = 2.95$ (case **N295**). According to [50], these choices describe stars with $\beta \sim 10^{-3} - 10^{-2}$, which correspond to $M \sim 10^4 - 10^5 M_{\odot}$, respectively. Their viscous timescales are computationally realizable with the resources available to us. To match the rotation profiles in [45,55], we choose the initial differential stellar rotation law as

$$u^t u_{\phi} = \frac{R_{\text{eq}}^2}{9} (\Omega - \Omega_c), \quad (16)$$

where $\Omega \equiv u^{\phi}/u^t$ is the angular velocity, and Ω_c is the angular velocity along the rotating axis. For nearly Newtonian configurations, the above rotation law reduces to

$$\Omega \approx \frac{\Omega_c}{1 + (9 + \varpi/R_{\text{eq}})^2}, \quad (\text{Newtonian}) \quad (17)$$

with $\varpi^2 = x^2 + y^2$. We set the ratio of the polar to equatorial radius to $R_{\text{pol}}/R_{\text{eq}} = 0.6$ and the central density low enough to guarantee dynamical radial stability. Both models have $T/|W| \approx 0.09$, which is both secularly and dynamically stable to the $m = 2$ mode, in contrast to the secularly unstable models with $T/|W| = 0.227$ in [45,55].

The star is seeded with a dipolelike, dynamically weak magnetic field confined to the stellar interior (see left panels in Fig. 1). The field is generated by the vector potential [49,50],

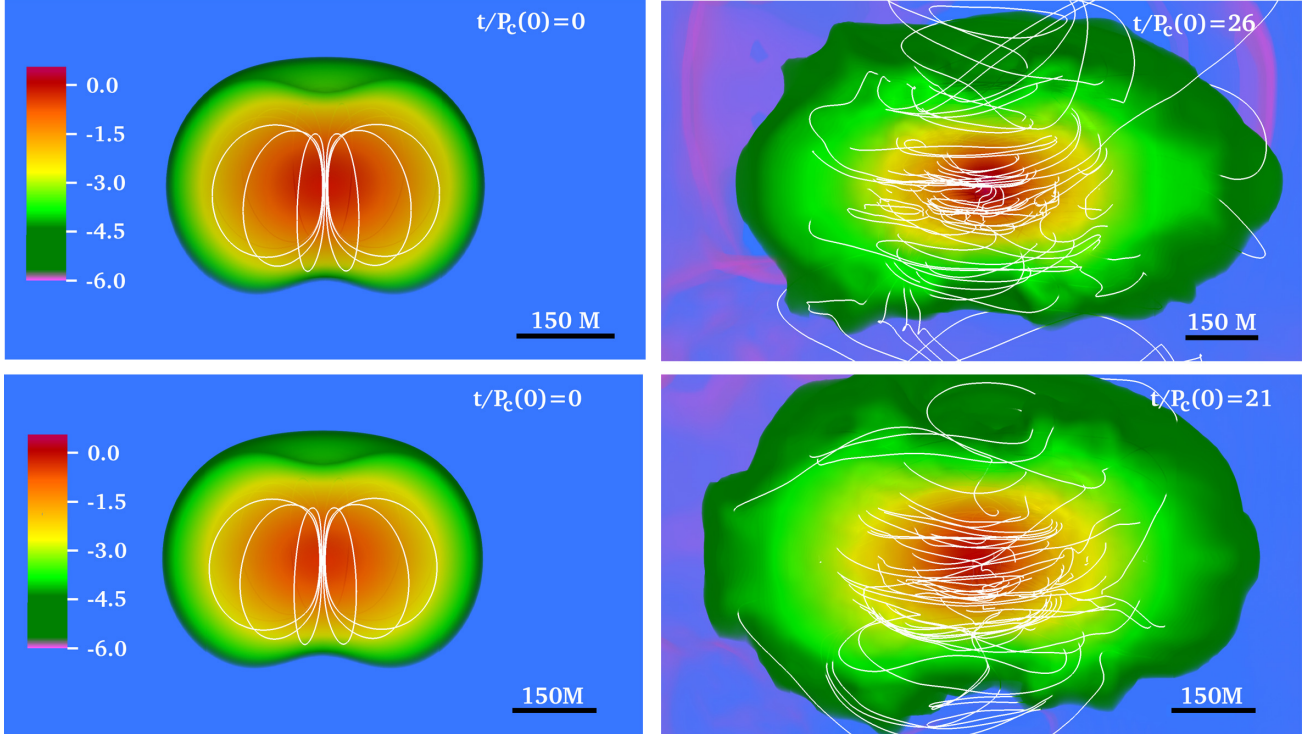


FIG. 1. Meridional cut through a 3D volume rendering of the rest-mass density, normalized to its initial maximum value $\rho_{0,\max}$ (log scale) for initial (left panels) and final configurations (right panels) for cases **N29** (top row) and **N295** (bottom row). For details see Table I. White solid lines denote the magnetic field lines. Here P_c denotes the initial central rotation period, which is $P_c = 8193M$ for **N29** and $P_c = 10582M$ for **N295**, with $M = 0.049(M/10^4 M_\odot) \text{ s} = 1.47 \times 10^4 (M/10^4 M_\odot) \text{ km}$.

$$A_\phi^{\text{int}} = A_b \varpi^2 \max(P - P_{\text{cut}}, 0)^{n_b}, \quad (18)$$

where A_b , P_{cut} , and n_b are constants that determine the strength, the degree of central condensation, and the confinement of the magnetic fields, respectively. Following [49,50], P_{cut} is set to 10^{-4} times the initial maximum value of the pressure and n_b to $1/8$. We then set the amplitude A_b such that $\mathcal{M}/W \approx 2.0 \times 10^{-4}$ for the two cases. The choice of the field strength is based on a compromise between insuring computationally achievable Alfvén and viscous damping timescales and preventing significant departures from hydrostatic equilibrium triggered by a dynamically strong magnetic field.

We cover the computational grid with a tenuous atmosphere with constant density $\rho_{0,\text{atm}} = 10^{-10} \rho_{0,\max}(0)$ following the standard setup in hydrodynamic and MHD

simulations, where $\rho_{0,\max}(0)$ is the maximum rest-mass density at $t = 0$. The key initial parameters are summarized in Tables I and II.

Before we start the numerical evolution of the above stars, we verify that MRI will be properly captured in our system. Following [40], we check that: (a) the magnetic field generated by the vector potential in Eq. (18) satisfies $\partial_\varpi \Omega < 0$, a condition need to trigger the instability. (b) The wavelength of the fastest-growing mode λ_{MRI} should be resolved by more than 10 grid points [63,69,70]. We plot the quality factor $Q = \lambda_{\text{MRI}}/dx$ on the equatorial plane, with dx the local grid spacing. As is shown in Fig. 2, we resolved λ_{MRI} by more than 15 grid points in the bulk of our stellar models except for the ring-shaped region where the magnetic field flips direction. (c) The wavelength λ_{MRI} should fit in the star. Figure 3 shows λ_{MRI} along with the rest-mass density on the meridional plane. It is clear that the

TABLE II. Initial model parameters. Here ρ_c denotes the central rest-mass density, R_{pol} is the polar radius, Ω_c is the central angular velocity, and $\langle B \rangle = \sqrt{8\pi\mathcal{M}/V_s}$ denotes the averaged magnetic field strength, where \mathcal{M} is the magnetic energy and $V_s = \int \sqrt{\gamma} d^3x$ is the initial proper volume of the star.

Case	ρ_c $[(M/10^4 M_\odot)^{-2} \text{ g cm}^{-3}]$	R_{pol} $[(M/10^4 M_\odot) \text{ cm}]$	Ω_c $[(M/10^4 M_\odot)^{-1} \text{ s}^{-1}]$	$\langle B \rangle$ $[(M/10^4 M_\odot)^{-1} \text{ G}]$
N29	4.23×10^3	2.38×10^{11}	0.016	2.68×10^9
N295	2.85×10^3	2.84×10^{11}	0.012	1.90×10^9

reaches a value of $\sim 2.5\%$ of the binding energy in case **N29** and $\sim 4.0\%$ in case **N295**. The internal energy E_{int} increases gradually with time, indicating continuous heating. The major heating energy coincides with the decrease of gravitational potential energy W due to the contraction of the stellar core [see Eq. (11)]. Note that, \mathcal{M} is not the main heating source because $\mathcal{M} \ll E_{\text{int}}$ throughout the evolution.

The rotational kinetic energy T , on the other hand, remains nearly constant throughout the whole simulation in **N29**, where we observe very small fractional changes. As shown in Fig. 4, after $t \gtrsim 20P_c$, the inner core remnant spins at $\sim 60\%$ of the initial angular velocity of the star. In contrast, T in **N295** increases by around 10% of its initial value. After $t \gtrsim 20P_c$, the inner core remnant spins at $\sim 66\%$ of the initial angular velocity of the star. Notice that the gravitational potential energy W decreases faster in **N295** than **N29**. This behavior suggests that the increase of T comes from W , indicating that the stiffer the EOS, the more difficult it is to transfer potential energy. These results display great differences from previous studies of magnetic braking of differential rotation in infinite cylinders and incompressible stars, where a substantial fraction of T is transferred to \mathcal{M} [56–58]. However, the energy evolution of our models shares several similarities with the B1 model in the study of magnetic braking and damping of neutron stars [62], where a nonhypermassive and “ultraspinning” (angular momentum exceeding the maximum for uniform rotation at the same rest mass) $\Gamma = 2$ polytrope with an effective turbulent viscosity were evolved.

VI. CONCLUSIONS

The growth of $m = 2$ seed density perturbations and their fragmentation in massive stars with a high degree of differential rotation undergoing collapse has been suggested as a viable channel for binary black hole formation. Here we illustrate the likely fate of such massive stars during their prior, stable, evolutionary lifetime. We build GR stellar models described by a polytropic EOS with polytropic index $n = 2.9$ and $n = 2.95$, with the same differential rotation law as in [45,54]. We endowed the stars with a dynamically weak, poloidal magnetic field confined to the stellar interior. The ratio of initial magnetic energy to gravitational potential energy is $\sim 2 \times 10^{-4}$.

We found that during the early phase of the evolution, magnetic winding and the MRI greatly amplify the initial magnetic field. During that period, the magnetic field is increased by ~ 50 times its initial value. At the same time, angular momentum from the inner layers of the star is transported outward. The inner layers then shrink and form a massive inner core in which the differential rotation eventually (around twenty rotation periods) is fully damped. Therefore, prior to reaching the state of gravitational radial instability, magnetic braking and turbulent magnetic viscosity drive a massive star to a new

quasiequilibrium state. This state consists of a uniformly rotating central core surrounded by a low-density Keplerian disk. These are not the matter or rotation profiles that will lead to growth and fragmentation of $m = 2$ density perturbations during catastrophic collapse.

We estimated various physical timescales that determine the stellar evolution of the stellar models considered here. Using the initial parameters of our GR stellar models, we found that the timescales obey a natural hierarchy [see Eq. (13)]. This hierarchy shows that during the normal evolutionary lifetime of a star, a sufficiently high degree of differential rotation required to trigger $m = 2$ perturbation growth and fragmentation leading to binary BH formation during collapse will be suppressed. Our numerical results should describe the fate of stars with characteristic masses greater than several hundred solar masses, which are possible progenitors of binary massive stellar-mass BHs and IMBHs that produce GW signals detectable by LVSC.

Given our numerical results, we conclude that the binary black hole formation channel described in [55] is not likely, assuming that the differentially rotating massive star that might undergo fragmentation during collapse experienced a long evolution phase in hydrostatic equilibrium before arriving at radial instability to collapse. During such a phase, even a small initial magnetic field will amplify and ultimately damp the differential rotation required to grow the $m = 2$ seed perturbations that trigger fission or fragmentation. However, if a high degree of differential rotation is resuscitated following some sudden catastrophic event, such as a massive star binary collision and merger, followed by a sudden collapse, then it may still be possible for the fragmentation-binary BH formation mechanism to be triggered. The likelihood of such an event remains to be determined.

We remark that the values of the α_{SS} parameter found numerically depend strongly on the adopted resolution. As it has been shown in [87–89] the higher the resolution, the higher the alpha parameter. Therefore, it is expected that in higher order numerical simulations the viscosity timescale, the time over which the turbulent viscosity damps differential rotation, will be shortened. But, magnetic winding and the MRI still will drive a massive star to a new quasiequilibrium state that consists of a uniformly rotating central core surrounded by a low-density Keplerian disk. Our basic conclusion during its lifetime therefore will remain unaffected, though the hierarchy of timescales in Eq. (13) may change.

ACKNOWLEDGMENTS

We thank V. Paschalidis for useful discussions and the Illinois Relativity group REU team (K. Nelli) for assistance in creating Fig. 1. This work has been supported in part by National Science Foundation (NSF) Grants No. PHY-1602536 and No. PHY-1662211, and NASA Grant No. 80NSSC17K0070 at the University of Illinois at

Urbana-Champaign. This work made use of the Extreme Science and Engineering Discovery Environment (XSEDE), which is supported by National Science Foundation Grant No. TG-MCA99S008. This research is part of the Blue Waters sustained-petascale computing

project, which is supported by the National Science Foundation (Grants No. OCI-0725070 and No. ACI-1238993) and the State of Illinois. Blue Waters is a joint effort of the University of Illinois at Urbana-Champaign and its National Center for Supercomputing Applications.

-
- [1] B. P. Abbott *et al.* (LIGO Scientific and Virgo Collaborations), *Phys. Rev. Lett.* **116**, 061102 (2016).
- [2] B. P. Abbott *et al.* (Virgo and LIGO Scientific Collaborations), *Phys. Rev. Lett.* **116**, 241103 (2016).
- [3] B. P. Abbott *et al.* (LIGO Scientific and Virgo Collaborations), *Phys. Rev. Lett.* **118**, 221101 (2017).
- [4] B. P. Abbott *et al.* (Virgo and LIGO Scientific Collaborations), *Phys. Rev. Lett.* **119**, 141101 (2017).
- [5] B. P. Abbott, R. Abbott, T. D. Abbott, F. Acernese, K. Ackley, C. Adams, T. Adams, P. Addesso, R. X. Adhikari, V. B. Adya *et al.*, *Astrophys. J. Lett.* **851**, L35 (2017).
- [6] B. P. Abbott *et al.* (Virgo and LIGO Scientific Collaborations), *arXiv:1811.12907*.
- [7] R. A. Remillard and J. E. McClintock, *Annu. Rev. Astron. Astrophys.* **44**, 49 (2006).
- [8] S. Bird, I. Cholis, J. B. Muñoz, Y. Ali-Haïmoud, M. Kamionkowski, E. D. Kovetz, A. Raccanelli, and A. G. Riess, *Phys. Rev. Lett.* **116**, 201301 (2016).
- [9] B. Carr, F. Kühnel, and M. Sandstad, *Phys. Rev. D* **94**, 083504 (2016).
- [10] S. Clesse and J. García-Bellido, *Phys. Dark Universe* **15**, 142 (2017).
- [11] Y. N. Eroshenko, *J. Phys. Conf. Ser.* **1051**, 012010 (2018).
- [12] S. L. Schröder, A. Batta, and E. Ramirez-Ruiz, *Astrophys. J. Lett.* **862**, L3 (2018).
- [13] A. V. Tutukov and L. R. YungelSon, *Mon. Not. R. Astron. Soc.* **260**, 675 (1993).
- [14] R. Voss and T. M. Tauris, *Mon. Not. R. Astron. Soc.* **342**, 1169 (2003).
- [15] S. E. Woosley, A. Heger, and T. A. Weaver, *Rev. Mod. Phys.* **74**, 1015 (2002).
- [16] K. Belczynski, T. Bulik, C. L. Fryer, A. Ruiter, F. Valsecchi, J. S. Vink, and J. R. Hurley, *Astrophys. J.* **714**, 1217 (2010).
- [17] M. Dominik, K. Belczynski, C. Fryer, D. E. Holz, E. Berti, T. Bulik, I. Mandel, and R. O’Shaughnessy, *Astrophys. J.* **779**, 72 (2013).
- [18] T. Kinugawa, K. Inayoshi, K. Hotokezaka, D. Nakauchi, and T. Nakamura, *Mon. Not. R. Astron. Soc.* **442**, 2963 (2014).
- [19] K. Belczynski, D. E. Holz, T. Bulik, and R. O’Shaughnessy, *Nature (London)* **534**, 512 (2016).
- [20] S. Stevenson, A. Vigna-Gmez, I. Mandel, J. W. Barrett, C. J. Neijssel, D. Perkins, and S. E. de Mink, *Nat. Commun.* **8**, 14906 (2013).
- [21] V. Kalogera, C. Kim, D. R. Lorimer, M. Burgay, N. D’Amico, A. Possenti, R. N. Manchester, A. G. Lyne, B. C. Joshi, M. A. McLaughlin *et al.*, *Astrophys. J. Lett.* **601**, L179 (2004).
- [22] P. Marchant, N. Langer, P. Podsiadlowski, T. M. Tauris, and T. J. Moriya, *Astron. Astrophys.* **588**, A50 (2016).
- [23] S. E. de Mink and I. Mandel, *Mon. Not. R. Astron. Soc.* **460**, 3545 (2016).
- [24] Note1, however, low-metallicity AGN is extremely rare from observations. For details, see, e.g., <http://dx.doi.org/10.1111/j.1365-2966.2006.10812.x>.
- [25] C. L. Rodriguez, M. Morscher, L. Wang, S. Chatterjee, F. A. Rasio, and R. Spurzem, *Mon. Not. R. Astron. Soc.* **463**, 2109 (2016).
- [26] S. Chatterjee, C. L. Rodriguez, and F. A. Rasio, *Astrophys. J.* **834**, 68 (2017).
- [27] M. Fishbach, D. E. Holz, and B. Farr, *Astrophys. J. Lett.* **840**, L24 (2017).
- [28] C. L. Rodriguez, C.-J. Haster, S. Chatterjee, V. Kalogera, and F. A. Rasio, *Astrophys. J. Lett.* **824**, L8 (2016).
- [29] M. C. Miller and E. J. M. Colbert, *Int. J. Mod. Phys. D* **13**, 1 (2004).
- [30] B. P. Abbott *et al.* (LIGO Scientific and Virgo Collaborations), *Phys. Rev. D* **96**, 022001 (2017).
- [31] J. R. Gair, I. Mandel, M. C. Miller, and M. Volonteri, *Gen. Relativ. Gravit.* **43**, 485 (2011).
- [32] V. Connaughton *et al.*, *Astrophys. J. Lett.* **826**, L6 (2016).
- [33] F. Verrecchia, M. Tavani, A. Ursi, A. Argan, C. Pittori, I. Donnarumma, A. Bulgarelli, F. Fuschino, C. Labanti *et al.*, *Astrophys. J. Lett.* **847**, L20 (2017).
- [34] M. Lyutikov, *arXiv:1602.07352*.
- [35] A. Khan, V. Paschalidis, M. Ruiz, and S. L. Shapiro, *Phys. Rev. D* **97**, 044036 (2018).
- [36] A. Loeb, *Astrophys. J. Lett.* **819**, L21 (2016).
- [37] J. M. Fedrow, C. D. Ott, U. Sperhake, J. Blackman, R. Haas, C. Reisswig, and A. De Felice, *Phys. Rev. Lett.* **119**, 171103 (2017).
- [38] L. Dai, J. C. McKinney, and M. C. Miller, *Mon. Not. R. Astron. Soc.* **470**, L92 (2017).
- [39] D. J. D’Orazio and A. Loeb, *Phys. Rev. D* **97**, 083008 (2018).
- [40] R. Gold, V. Paschalidis, Z. B. Etienne, S. L. Shapiro, and H. P. Pfeiffer, *Phys. Rev. D* **89**, 064060 (2014).
- [41] R. Gold, V. Paschalidis, M. Ruiz, S. L. Shapiro, Z. B. Etienne, and H. P. Pfeiffer, *Phys. Rev. D* **90**, 104030 (2014).
- [42] T. W. Baumgarte and S. L. Shapiro, *Astrophys. J.* **526**, 941 (1999).
- [43] M. Shibata and S. L. Shapiro, *Astrophys. J. Lett.* **572**, L39 (2002).
- [44] M. Saijo, T. W. Baumgarte, S. L. Shapiro, and M. Shibata, *Astrophys. J.* **569**, 349 (2002).

- [45] B. Zink, N. Stergioulas, I. Hawke, C. D. Ott, E. Schnetter, and E. Müller, *Phys. Rev. Lett.* **96**, 161101 (2006).
- [46] M. Saijo and I. Hawke, *Phys. Rev. D* **80**, 064001 (2009).
- [47] M. Shibata, H. Uchida, and Y. Sekiguchi, *Astrophys. J.* **818**, 157 (2016).
- [48] S. P. Butler, A. R. Lima, T. W. Baumgarte, and S. L. Shapiro, *Mon. Not. R. Astron. Soc.* **477**, 3694 (2018).
- [49] L. Sun, V. Paschalidis, M. Ruiz, and S. Shapiro, *Phys. Rev. D* **96**, 043006 (2017).
- [50] L. Sun, M. Ruiz, and S. Shapiro, *Phys. Rev. D* **98**, 103008 (2018).
- [51] P. Bodenheimer and J. P. Ostriker, *Astrophys. J.* **180**, 159 (1973).
- [52] K. C. B. New and S. L. Shapiro, *Classical Quantum Gravity* **18**, 3965 (2001).
- [53] K. C. B. New and S. L. Shapiro, *Astrophys. J.* **548**, 439 (2001).
- [54] B. Zink, N. Stergioulas, I. Hawke, C. D. Ott, E. Schnetter, and E. Müller, *Phys. Rev. D* **76**, 024019 (2007).
- [55] C. Reisswig, C. Ott, E. Abdikamalov, R. Haas, P. Moesta, and E. Schnetter, *Phys. Rev. Lett.* **111**, 151101 (2013).
- [56] S. L. Shapiro, *Astrophys. J.* **544**, 397 (2000).
- [57] J. N. Cook, S. L. Shapiro, and B. C. Stephens, *Astrophys. J.* **599**, 1272 (2003).
- [58] Y. T. Liu and S. L. Shapiro, *Phys. Rev. D* **69**, 044009 (2004).
- [59] Z. B. Etienne, Y. T. Liu, and S. L. Shapiro, *Phys. Rev. D* **74**, 044030 (2006).
- [60] M. D. Duez, Y. T. Liu, S. L. Shapiro, and B. C. Stephens, *Phys. Rev. D* **69**, 104030 (2004).
- [61] M. D. Duez, Y. T. Liu, S. L. Shapiro, M. Shibata, and B. C. Stephens, *Phys. Rev. Lett.* **96**, 031101 (2006).
- [62] M. D. Duez, Y. T. Liu, S. L. Shapiro, M. Shibata, and B. C. Stephens, *Phys. Rev. D* **73**, 104015 (2006).
- [63] M. Shibata, Y. T. Liu, S. L. Shapiro, and B. C. Stephens, *Phys. Rev. D* **74**, 104026 (2006).
- [64] R. F. Penna, J. C. McKinney, R. Narayan, A. Tchekhovskoy, R. Shafee, and J. E. McClintock, *Mon. Not. R. Astron. Soc.* **408**, 752 (2010).
- [65] T. W. Baumgarte and S. L. Shapiro, *Numerical Relativity: Solving Einstein's Equations on the Computer* (Cambridge University Press, Cambridge, England, 2010).
- [66] G. B. Cook, S. L. Shapiro, and S. A. Teukolsky, *Astrophys. J.* **398**, 203 (1992).
- [67] G. B. Cook, S. L. Shapiro, and S. A. Teukolsky, *Astrophys. J.* **422**, 227 (1994).
- [68] G. B. Cook, S. L. Shapiro, and S. A. Teukolsky, *Astrophys. J.* **424**, 823 (1994).
- [69] T. Sano, S.-i. Inutsuka, N. J. Turner, and J. M. Stone, *Astrophys. J.* **605**, 321 (2004).
- [70] H. Shiokawa, J. C. Dolence, C. F. Gammie, and S. C. Noble, *Astrophys. J.* **744**, 187 (2012).
- [71] Note2, <http://www.cactuscode.org>.
- [72] Note3, <http://www.carpetcode.org>.
- [73] M. Shibata and T. Nakamura, *Phys. Rev. D* **52**, 5428 (1995).
- [74] T. W. Baumgarte and S. L. Shapiro, *Phys. Rev. D* **59**, 024007 (1998).
- [75] J. G. Baker, J. Centrella, D.-I. Choi, M. Koppitz, and J. van Meter, *Phys. Rev. Lett.* **96**, 111102 (2006).
- [76] M. Campanelli, C. O. Lousto, P. Marronetti, and Y. Zlochower, *Phys. Rev. Lett.* **96**, 111101 (2006).
- [77] I. Hinder, A. Buonanno, M. Boyle, Z. B. Etienne, J. Healy *et al.*, *Classical Quantum Gravity* **31**, 025012 (2014).
- [78] M. Ruiz, D. Hilditch, and S. Bernuzzi, *Phys. Rev. D* **83**, 024025 (2011).
- [79] Z. B. Etienne, V. Paschalidis, Y. T. Liu, and S. L. Shapiro, *Phys. Rev. D* **85**, 024013 (2012).
- [80] Z. B. Etienne, Y. T. Liu, and S. L. Shapiro, *Phys. Rev. D* **82**, 084031 (2010).
- [81] M. D. Duez, Y. T. Liu, S. L. Shapiro, and B. C. Stephens, *Phys. Rev. D* **72**, 024028 (2005).
- [82] B. D. Farris, R. Gold, V. Paschalidis, E. Z. B., and S. Shapiro, *Phys. Rev. Lett.* **109**, 221102 (2012).
- [83] V. Paschalidis, Z. B. Etienne, and S. L. Shapiro, *Phys. Rev. D* **88**, 021504 (2013).
- [84] Z. B. Etienne, J. A. Faber, Y. T. Liu, S. L. Shapiro, K. Taniguchi, and T. W. Baumgarte, *Phys. Rev. D* **77**, 084002 (2008).
- [85] Z. B. Etienne, Y. T. Liu, S. L. Shapiro, and T. W. Baumgarte, *Phys. Rev. D* **79**, 044024 (2009).
- [86] M. Shibata, *100 Years of General Relativity* (World Scientific, Singapore, 2015).
- [87] K. Kiuchi, K. Kyutoku, Y. Sekiguchi, and M. Shibata, *Phys. Rev. D* **97**, 124039 (2018).
- [88] J. F. Hawley, S. A. Richers, X. Guan, and J. H. Krolik, *Astrophys. J.* **772**, 102 (2013).
- [89] J. F. Hawley, X. Guan, and J. H. Krolik, *Astrophys. J.* **738**, 84 (2011).